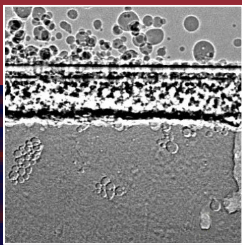

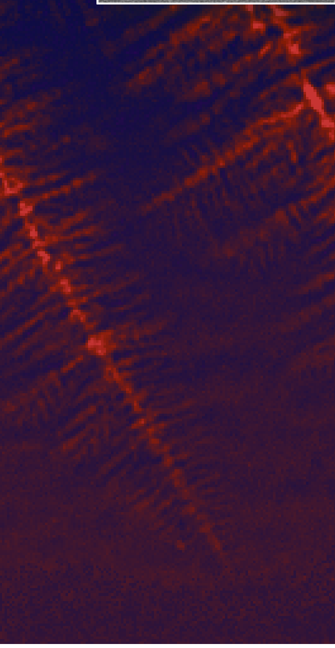

In situ/operando synchrotron x-ray studies of metal additive manufacturing

Tao Sun, Wenda Tan, Lianyi Chen, and Anthony Rollett

Additive manufacturing (AM) comprises a group of transformative technologies that are likely to revolutionize manufacturing. In particular, laser-based metal AM techniques can not only fabricate parts with extreme complexity, but also provide innovative means for designing and processing new metallic systems. However, there are still several technical barriers that constrain metal AM. Overcoming these barriers requires a better understanding of the physics underlying the complex and dynamic laser–metal interaction at the heart of many AM processes. This article briefly describes the state of the art of *in situ/operando* synchrotron x-ray imaging and diffraction for studying metal AM, mostly the laser powder-bed fusion process. It highlights the immediate impact of *operando* synchrotron studies on the advancement of AM technologies, and presents future research challenges and opportunities.

Introduction

Powder-bed additive manufacturing (AM) processes join material layer-by-layer to make three-dimensional parts from computer models. AM exhibits many advantages over subtractive and formative manufacturing technologies, such as increased part complexity, high customization, short supply chain, on-site and on-demand production, reduction of material and energy consumption. Since AM largely unleashes the freedom to design, topologically optimized parts can now be built with superior performance that were previously inaccessible.[1,2] In both the public and private sectors, metal AM has evolved from a rapid prototyping tool to a full-scale product manufacturing technology in the past decade, and has found many applications in aerospace, automobile, medical, defense, and energy industries. Meanwhile, metallurgists have been tackling the tremendous challenges in metal AM and seizing opportunities for fundamental research for designing and processing new alloys and metallic architectures.[3–6] Owing to the rapid melting and solidification characteristics of AM, the printed metals exhibit unique microstructures, such as cellular structures, high dislocation densities, solute trapping, unusual chemical segregation, porosity, and nonequilibrium phases.[7–14] Some of these structural attributes are favorable for certain applications, while others are deleterious.

Understanding the process–structure–property relationship in AM metals is key to avoiding detrimental defect structures and improving the reliability of printed parts. In an earlier issue of *MRS Bulletin*, five articles reviewed the unique microstructures (characterized primarily using *ex situ* techniques) and properties of different alloys processed using AM techniques.[15] In this article, we introduce remaining materials issues in metal AM and highlight the recent development of *in situ/operando* synchrotron x-ray experiments for probing the dynamic energy-matter interaction involved in powder-bed AM and the microstructure evolution during the rapid cooling process. The article ends with a discussion on future research opportunities.

Key processes in laser powder-bed fusion

Laser powder-bed fusion (LPBF) is currently the dominant metal AM technique. In a typical LPBF process, as schematically shown in **Figure 1**, a laser selectively illuminates certain locations on the powder bed to melt the powder and underlying substrate and create a melt pool. Under most build conditions, the laser power is high enough to induce metal evaporation. The metal vapor leaves the melt pool surface with a high speed and creates a recoil pressure that pushes the liquid metal away to form a depression zone. The high-speed vapor jet may also impact on other regions of the depression zone to modify the local fluid flow and interface shape. The general shape of the depression zone varies with the laser parameters (i.e., power and scanning speed), and it often fluctuates with various

Tao Sun, Department of Materials Science and Engineering, University of Virginia, USA; ts7qw@virginia.edu
Wenda Tan, Department of Mechanical Engineering, The University of Utah, USA; wenda.tan@mech.utah.edu
Lianyi Chen, Department of Mechanical Engineering, University of Wisconsin–Madison, USA; lianyi.chen@wisc.edu
Anthony Rollett, Department of Materials Science and Engineering, Carnegie Mellon University, USA; rollett@andrew.cmu.edu
doi:10.1557/mrs.2020.275

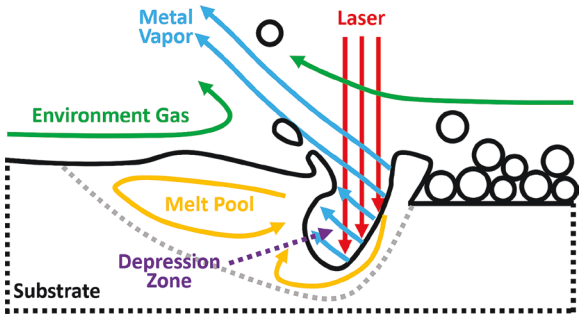

Figure 1. Schematic illustration of the physical processes involved in laser powder-bed fusion.

magnitudes during the laser scanning. Multiple reflection of the laser can occur inside the depression zone, which leads to an increase in overall laser absorption by the material, yet resulting in nonuniform local absorption.

Dynamic fluid flow exists in both the gas region and the melt pool. In the gas region, the high-speed vapor flow drives the environment gas right above the powder bed to flow toward the jet, which causes the local powder particles to move toward the vapor jet as well (i.e., powder entrainment). Once the particles move close to the vapor jet, they will be pushed away by the jet with a high speed (i.e., powder ejection). Inside the melt pool, the liquid metal flow is driven by a combination of multiple forces, including vaporization-induced recoil pressure, the impact pressure by the high-speed metal vapor, the Laplace pressure, and thermocapillary stress due to the surface tension on the melt pool surface. These forces create a complex flow pattern with multiple vortices inside the melt pool.

The dynamic fluctuation of the depression zone and the multiphase fluid flow are highly coupled during the laser–metal interaction. As the depression zone changes its transient shape, the spatial distribution of laser absorption varies and induces evaporation at different locations with different intensities. This can considerably alter the fluid flow patterns in both the gaseous region and the melt pool, which, in turn, can modify the shape of the depression zone. The powder-bed configuration and powder motion also introduce certain randomness in the laser absorption, as well as the distributions of energy, mass, and mechanical forces. Collectively, these factors make this multiphysics process even more dynamic and unstable.

The dynamic fluctuation of the depression zone and intense melt flow lead to dynamic change of the melt pool geometry, and thereby the local solidification velocity. However, the influence of the melt pool fluctuation on the solidification behavior and material microstructure is still largely unknown. Furthermore, rapid solidification may induce a complex solid–liquid interface because of the high interface mobility compared to the local diffusion. The local solute partitioning can lead to spatial variation in constitutional undercooling. This may affect the phase and grain morphological evolution and form kinetically favored metastable structures. High-speed x-ray imaging and diffraction may be a powerful tool to understand these complex processes.

Operando synchrotron x-ray imaging of metal AM

At the Advanced Photon Source (APS) of Argonne National Laboratory, we innovated an experimental platform for *operando* studies of metal AM processes. The superior penetration power of high-energy x-rays and the extremely high photon flux afforded by the third-generation synchrotron facility allow the quantitative characterization of dynamic structural evolution in bulk metallic materials with unprecedented spatial and temporal resolutions. *Operando* high-speed x-ray imaging experiments on LPBF (presented in this contribution) were performed at the 32-ID-B beamline of the APS. **Figure 2**a shows the schematic and a photograph of the beamline setup, with details reported previously.[16,17] The minimum spatial resolution is 1 µm, maximum frame rate is

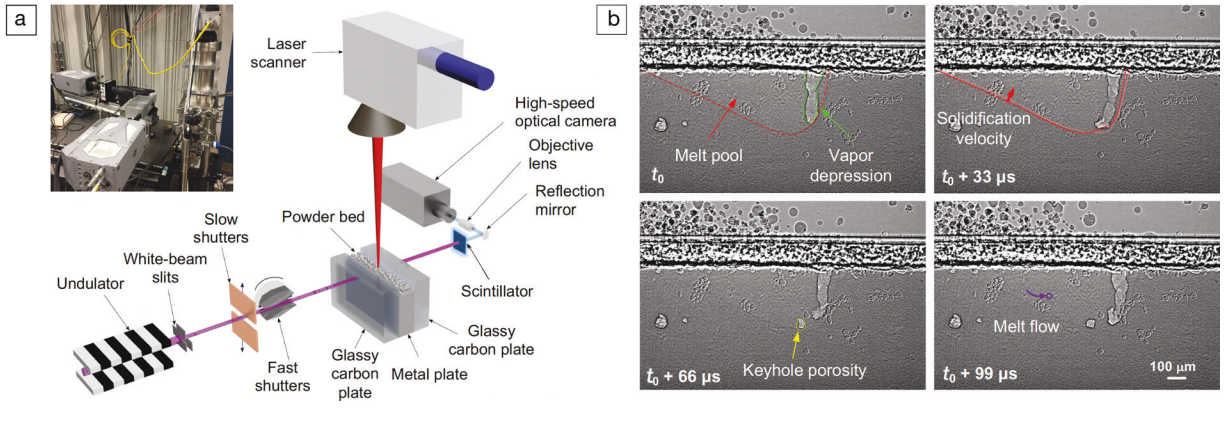

Figure 2. (a) Photograph and schematic of *operando* synchrotron x-ray experiment on laser powder-bed fusion (LPBF). (b) Representative x-ray images of the LPBF process of AlSi10Mg. The frame rate is 30,173 fps, and the exposure time for each image is ~100 ps (i.e., a single x-ray pulse).

6.5 MHz, and minimum temporal resolution is 100 ps (i.e., a single x-ray pulse). In the experiment, the laser is scanned in straight-line motion across the powder bed sample and x-rays penetrate from the side providing a view in which the powder bed is on top and the metal substrate is at the bottom. A representative case of *operando* x-ray imaging is present in Figure 2b, in which the LPBF process of AlSi10Mg with the laser power 540 W, scan speed 0.6 m/s, and laser spot size 100 µm is revealed. With the high resolution and the decent contrast between the vapor, liquid, and solid phases, many significant structure parameters in LPBF can be precisely measured, such as the melt pool and vapor depression morphologies, solidification rate, melt flow, and spatter trajectory.

Understanding defect generation and elimination mechanisms

Internal defects (e.g., voids, pores, cracks) are commonly observed in AM metals,[6] which severely deteriorate their properties, especially the fatigue life.[18] Due to the challenge of studying the defect formation mechanisms by postmortem microstructure analysis, *operando* synchrotron x-ray imaging technique, illustrated in Figure 2, was demonstrated to be a powerful tool to observe the transient dynamics of defect formation and evolution in real time. The deeper understanding gained from *operando* experiments will provide the foundation for designing defect mitigation and elimination approaches for achieving defect-less products via metal AM.

High-speed high-resolution x-ray imaging investigations have revealed various pore formation mechanisms during the LPBF process of TiAl6V4 and AlSi10Mg: transfer of pore from feedstock powders (**Figure 3**a),[19,20] pore formation due to vapor cavity instabilities,[21–25] pores generated by the vaporization of volatile substance or expansion of trapped gas,[20,26] porosity induced by melt pool surface fluctuations,[20] and pores forming from cracks.[20] Understanding how pores evolve after their formation is critical for designing pore mitigation strategies to eliminate various pores introduced into the melt pool. The high spatial and temporal resolutions afforded by the APS enables the direct observation of the highly dynamic and complex pore motions in the melt pool.[16] Figure 3b reveals the dynamic evolution of pores at different regions of the melt pool in AlSi10Mg, induced by laser rescanning. At the laser-interaction region (bottom panel of Figure 3b), a thermocapillary force driven pore elimination mechanism was discovered, leading to the design of a pore elimination strategy for achieving pore-free build via LPBF with powder feedstock containing substantial trapped gas pores (an example in TiAl6V4 in Figure 3c).

Cracking is another defect that occurs in some printed metals and is generally highly detrimental to ductility in particular. Recently, *operando* high-speed x-ray imaging was used to capture the transient dynamics of hot cracking during laser melting of aluminum alloy 6061. The initiation of hot cracking from a trapped bubble and crack healing by backfilling of liquid were observed. The feasibility of determining the point of origin for hot cracking was also demonstrated.[27]

Inform, validate, and calibrate numerical models

Operando synchrotron x-ray imaging has provided unprecedented information for the calibration and development of various numerical models for process dynamics.[21,24,28]

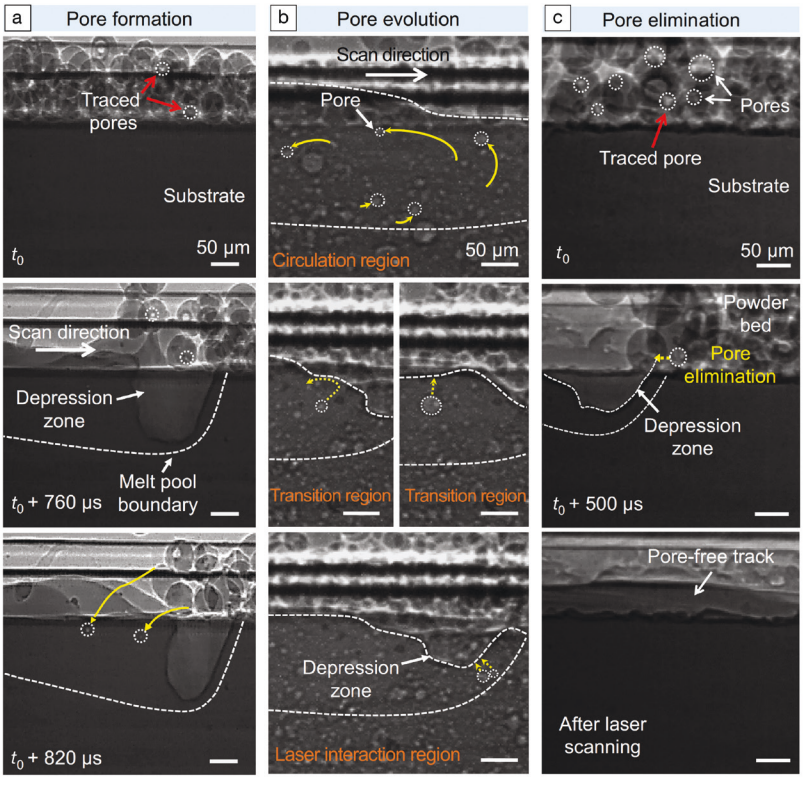

Figure 3. Defect generation and elimination mechanisms revealed by *operando* synchrotron x-ray imaging. (a) Pore transfer from feedstock powders to melt pool during laser powder-bed fusion (LPBF) of TiAl6V4. (b) Pore evolution dynamics during LPBF of AlSi10Mg. Pores follow circular patterns at the circulation region (top), while pores in the laser interaction region move toward the depression zone and escape from the melt pool (bottom). In the transition domain (middle), pores exhibit irregular motions, sometimes circulating in the melt pool, and sometimes moving toward the melt pool surface and escaping. (c) Pore elimination in TiAl6V4 using thermocapillary force.[15,16] Adapted with permission from Reference 20. © 2019 Springer Nature.

Specifically, the actual geometry of the depression zone and its dynamic fluctuation, which are hidden in the center of the optically opaque substrate, can be revealed and measured with high spatial and temporal resolutions. The fluid flow in the melt pool can also be quantified by embedding microparticles into the sample as tracers.[29] These microtracers are generally refractory materials with much higher melting point than the metal being processed and different density to yield good contrast in x-ray images. Such experimental data provide the ground truth for different process dynamic models as benchmarks. Once validated, these models can in turn provide detailed information for the physical quantities of interest that are difficult to measure experimentally, such as the temperature distribution and various mechanical forces inside the melt pool. Collectively, x-ray imaging and simulations provide a comprehensive description of the physics in the metal AM process.

The basic step for validating a process model is to check its prediction for the quasi-steady state of the process. The simulation results of the general size of the depression zone and melt pool as well as the melt flow velocity can be directly compared with x-ray measurements. The more advanced step of model validation is to check the model predictions for transient phenomena, such as the initial drilling of the depression zone, pore formation, and particle spattering. For these processes, the simulation should provide reasonable numerical description not only for the magnitudes of relevant physical quantities, but also their temporal and spatial variations. *Operando* x-ray imaging is capable of capturing these highly dynamic processes, which prompts further development of fundamental theories and sophisticated multiphysics models.[30,31]

X-ray imaging also provides valuable information to the computational materials models of the microstructure evolution during metal solidification. There have been efforts to inform or calibrate phase-field[32] and cellular automata[33] models using the x-ray imaging results for the slow solidification processes (i.e., casting). For the metal AM process, the solidification front velocity can be accurately measured using x-ray imaging, which can potentially be used to inform and validate the solidification models. However, further details of the rapid solidified microstructure in the metal AM are beyond the spatial resolution (i.e., 1 μm) of the current high-speed x-ray imaging capability.

Support development of process monitoring and control systems

LPBF is extremely sensitive to many seemingly unimportant but practical factors (e.g., degradation of laser power, drifting of laser beam size on sample, defective optics, and storage condition for the powder feedstock). These strongly influence the reliability and repeatability issue of AM systems, for example, the same parameter set may not yield the same build quality by different machines or even by the same machine at different times. To address this issue, there have been substantial efforts worldwide devoted to the development of in-process monitoring and closed-loop control systems. These systems aim for detecting build anomalies in real time, analyzing the situation, and making the decision either to stop the process, or continue the process while creating a log file to facilitate the post-examination of the part, or generate a new parameter set for fixing the errors. Currently, the commonly used sensory devices are visible-light and thermal cameras, and ultrasound sensors. Since optical imaging can only capture the sample information on or above the surface, their fidelity for capturing defect formation inside the sample is relatively low. Ultrasound signals may reflect changes in the sample internal structures, but they can be challenging to interpret. Therefore, *operando* x-ray imaging has been used to calibrate these sensors by providing unambiguous information on the morphology of the vapor depression and melt pool, as well as the size and location of internal defects.[34–36]

Operando synchrotron x-ray imaging of other metal AM processes

In addition to LPBF, *operando* synchrotron x-ray imaging is also used for studying other metal AM processes, including blown-powder directed energy deposition (DED) and binder jetting. Both of these metal AM techniques have their own advantages and niche applications. Blown-powder laser DED adds flexibility for controlling the local composition of the complex build, while binder jetting decouples the printing process and subsequent densification post-processing step, so thermal residual stresses and highly anisotropic microstructures can be avoided.

In a previous study, a gravity-fed, low powder mass flow DED system was integrated into the high-speed x-ray imaging beamline.[37] Particles that flow into the melt pool influence the stability of the vapor depression and the surrounding melt pool, which increases the chance of porosity generation. The pore formation mechanism unique to the blown-powder DED process is being systematically investigated at the APS using an *operando* system equipped with commercial gas nozzles.[38] For studying binder jetting, a commercial system with droplet-on-demand ink-jet printhead was employed in the *operando* synchrotron x-ray imaging experiment.[39] The impact of the high-velocity droplet on the powder bed causes movement and ejection of the powder particles. The depth of disturbance is dependent on the size, shape, and material of the powder particles. The large volume of ejected particles left a depleted zone in the wake of the binder. Both subsurface motion and ejection of particles can potentially increase porosity in the printed parts.

In situ synchrotron x-ray diffraction of rapid melting and solidification of metals

The full-field optics-free x-ray imaging technique relies on the density difference to generate contrast. The highest resolution now is 1 μm, which is limited collectively by the wavelength of the visible light emitted by the scintillators, the x-ray source size, the source-to-sample distance, and the pixel size of the

optical sensors. Therefore, the high-speed x-ray imaging is not sensitive to the grain morphology and texture, dislocation networks, nanoscale chemical segregation, or atomic structure of a metal sample. X-ray diffraction, on the other hand, can provide direct or indirect information on these important structural attributes.

At the APS, *in situ* diffraction experiments were carried out at multiple beamlines to study the rapid laser melting and solidification of metals. **Figure 4**a–b shows the representative 32-ID and 1-ID *in situ* diffraction data of laser melting of TiA16V4 plates, respectively. The 32-ID beamline uses undulator "pink" beams for diffraction experiments (first harmonic around 24 keV). With the absence of monochromator and major optics, the flux of the incident beam is preserved, so a much higher temporal resolution can be achieved. A home-integrated scintillator-based detector is used for collecting the diffraction patterns with a frame rate up to 2 MHz.[40] A tradeoff for the high temporal resolution is the low resolution in reciprocal space (i.e., scattering vector q) due to the large energy bandwidth of the incident beam (i.e., 10^{-2}) and the low dynamic range of the diffraction data. Six frames are selected to reveal the melting, solidification, and phase transformation process of TiA16V4 (i.e., fine α → melting → coarse β → fine α) in Figure 4a. The laser power is 440 W, scan speed is 1.2 m/s, and laser spot size is 100 µm. 1-ID is a high-energy monochromatic x-ray diffraction beamline (E = 55.6 keV in Figure 4b). A PILATUS3X 2M CdTe pixel array detector is used in the diffraction experiments. The high sensitivity and counter depth of the detector, coupled with the high q resolution afforded by the small energy bandwidth (i.e., 10^{-4}) of the monochromatic beam, allow the detection of both main and minor phases in materials simultaneously without changing the exposure time setting.[41] This is evidenced in Figure 4b, in which the β phase (less than 5%) in the sample before laser melting can be readily characterized with 2 ms detector exposure time. Given their unique advantages and limitations, these two diffraction techniques are highly complementary, and thereby can be applied for studying different structural dynamics involved in metal AM.

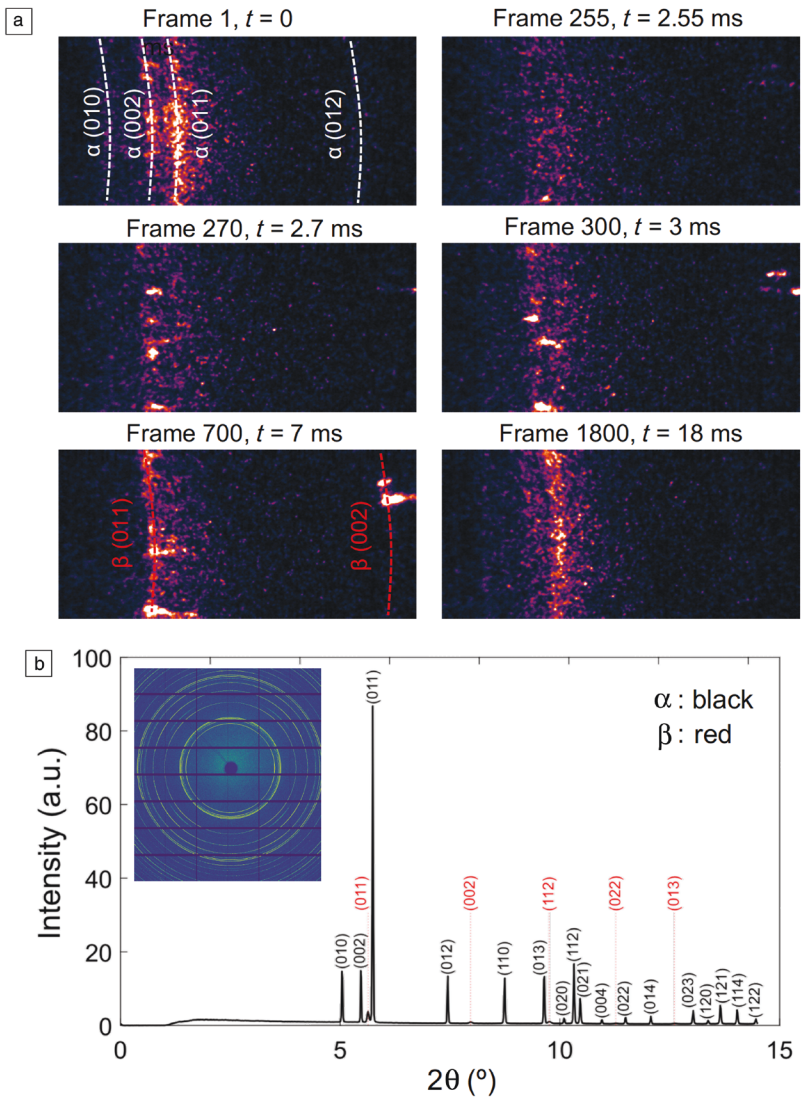

Figure 4. Representative *in situ* x-ray diffraction data collected at the Advanced Photon Source (a) 32-ID and (b) 1-ID beamlines from TiAl6V4 plate samples. The raw data at the 32-ID beamline were collected with a frame rate of 100 kHz and an exposure time of 5 µs, and data at the 1-ID beamline were collected with a frame rate of 250 Hz and an exposure time of 2 ms.

Future perspectives

The last few years have seen a rapid growth of the research community that applies *in situ*/*operando* synchrotron techniques for AM studies. There are vibrant research activities at several synchrotron facilities across the world, including the Stanford Synchrotron Radiation Lightsource (SSRL),[25,42–44] Diamond Light Source (DLS),[26,45,46] European Synchrotron Radiation Facility (ESRF),[47] and Swiss Light Source (SLS).[48–50] New insights gained from synchrotron studies have substantially advanced the field of metal AM. Over the next decade, most of these facilities will undergo major upgrades to diffraction-limited sources. The spatial and temporal resolutions and sensitivity of full-field imaging will be dramatically enhanced. Meanwhile, the small source size will markedly increase the flux of a focused beam, benefiting the *in situ*

diffraction experiments. One can reasonably expect to be able to probe many more details of the aforementioned dynamic processes (particularly for high-*Z* materials) and also study other phenomena in metal AM, such as chemical segregation during solidification, precipitation below a micron, transitions of minor phases on a microsecond time scale. Along with the source and beamline development, more sophisticated AM apparatus are highly desirable for the next generation of *operando* x-ray experiments. These systems must emulate the real AM processes with higher fidelity, integrate with more advanced sensors, provide more controls for the printing process, and allow faster sample switching and data collection.

With the rapidly increasing number of *in situ*/*operando* synchrotron experiments being carried out, another set of challenges emerges, namely, data collection, storage, transfer, and analysis. The popular perception of the data challenge focuses on how to exploit large sets of data such as photographs, diffractograms and videos. The inherent assumption is that such images are complex but sufficiently information rich that patterns can be discovered automatically via machine learning and not necessarily with any human intervention. The data challenges in the context of x-ray imaging and diffraction are quite other than this, in terms of raw data processing, information extraction and interpretation as follows. The data set from any given experiment is large, for example, many gigabytes, and the image generation physics is generally well enough understood to permit forward modeling. Extracting useful information at the required high precision is, however, a different task from distinguishing cars from cats. Moreover, the data rate is increasing to the point where special computers will be required to capture all the raw data or process it on-the-fly.[51] For x-ray imaging, there are many features such as pore formation that would be useful to be able to detect and quantify in a sufficiently automatic way that large numbers of experiments could be efficiently analyzed: with the low contrast available with dense metals, including many of those of practical interest such as steels and nickel alloys, this offers challenges aplenty for image processing, for example.

In summary, *in situ*/*operando* synchrotron x-ray study of metal AM is still in its infancy. While tremendous progress has been made in the last few years and remarkable insights have been gained, there are still many challenges and opportunities in this research field, which demands substantial efforts by scientists and engineers in academia, government laboratories, and industry.

Acknowledgments

We are pleased to acknowledge our many colleagues for their contributions to the *in situ*/*operando* synchrotron studies described herein, including C. Zhao, N. Parab, S. Wolff, B. Gould, N. Kouraytem, X. Li, Q. Guo, L. Escano, S.M. Hojjatzadeh, M. Qu, L. Xiong, R. Cunningham, C. Kantzos, and J. Pauza. We also thank K. Fezzaa and C.-P. Chuang for their support on the beamline experiments. W.T. acknowledges support from the National Science Foundation (NSF) (Award Nos. 1752218 and 1933368). L.C. acknowledges support from the NSF (Award Nos. 2002840 and 2011354). A.D.R. acknowledges support from the National Nuclear Security Administration under Grant No. DE-NA0003915. Synchrotron experiments described in this contribution used resources of the Advanced Photon Source, a US Department of Energy (DOE) Office of Science User Facility operated for the DOE Office of Science by Argonne National Laboratory under Contract No. DE-AC02–06CH11357.

References

1. S.H. Huang, P. Liu, A. Mokasdar, L. Hou, *Int. J. Adv. Manuf. Technol.* **67**, 1191 (2013).
2. W.E. Frazier, *J. Mater. Eng. Perform.* **23**, 1917 (2014).
3. D.D. Gu, W. Meiners, K. Wissenbach, R. Poprawe, *Int. Mater. Rev.* **57**, 133 (2012).
4. W.E. King, A.T. Anderson, R.M. Ferencz, N.E. Hodge, C. Kamath, S.A. Khairallah, A.M. Rubenchik, *Appl. Phys. Rev.* **2**, 041304 (2015).
5. W.J. Sames, F.A. List, S. Pannala, R.R. Dehoff, S.S. Babu, *Int. Mater. Rev.* **61**, 315 (2016).
6. T. DebRoy, H.L. Wei, J.S. Zuback, T. Mukherjee, J.W. Elmer, J.O. Milewski, A.M. Beese, A. Wilson-Heid, A. De, W. Zhang, *Prog. Mater. Sci.* **92**, 112 (2018).
7. M.J. Aziz, *J. Appl. Phys.* **53**, 1158 (1982).
8. P.M. Smith, M.J. Aziz, *Acta Metall. Mater.* **42**, 3515 (1994).
9. J.A. Kittl, P.G. Sanders, M.J. Aziz, D.P. Brunco, M.O. Thompson, *Acta Mater.* **48**, 4797 (2000).
10. T. Pinomaa, N. Provatas, *Acta Mater.* **168**, 167 (2019).
11. Y.M. Wang, T. Voisin, J.T. McKeown, J. Ye, N.P. Calta, Z. Li, Z. Zeng, Y. Zhang, W. Chen, T.T. Roehling, R.T. Ott, M.K. Santala, P.J. Depond, M.J. Matthews, A.V. Hamza, T. Zhu, *Nat. Mater.* **17**, 63 (2018).
12. B. Dovgyy, P.A. Hooper, C.M. Gourlay, A. Piglione, *Nat. Commun.* **11**, 1 (2020).
13. J.H. Martin, B.D. Yahata, J.M. Hundley, J.A. Mayer, T.A. Schaedler, T.M. Pollock, *Nature* **549**, 365 (2017).
14. D. Zhang, D. Qiu, M.A. Gibson, Y. Zheng, H.L. Fraser, D.H. St. John, M.A. Easton, *Nature* **576**, 91 (2019).
15. S. Das, D.L. Bourell, S.S. Babu, *MRS Bull.* **41**, 729 (2016).
16. C. Zhao, K. Fezzaa, R.W. Cunningham, H. Wen, F. De Carlo, L. Chen, A.D. Rollett, T. Sun, *Sci. Rep.* **7**, 1 (2017).
17. N.D. Parab, C. Zhao, R. Cunningham, L.I. Escano, K. Fezzaa, W. Everhart, A.D. Rollett, L. Chen, T. Sun, *J. Synchrotron Radiat.* **25**, 1467 (2018).
18. S. Leuders, M. Thöne, A. Riemer, T. Niendorf, T. Tröster, H.A. Richard, H.J. Maier, *Int. J. Fatigue* **48**, 300 (2013).
19. A. Bobel, L.G. Hector, I. Chelladurai, A.K. Sachdev, T. Brown, W.A. Poling, R. Kubic, B. Gould, C. Zhao, N. Parab, A. Greco, T. Sun, *Materialia* **6**, 100306 (2019).
20. S.M.H. Hojjatzadeh, N.D. Parab, Q. Guo, M. Qu, L. Xiong, C. Zhao, L.I. Escano, K. Fezzaa, W. Everhart, T. Sun, L. Chen, *Int. J. Mach. Tools Manuf.* **153**, 103555 (2020).
21. S.M.H. Hojjatzadeh, N.D. Parab, W. Yan, Q. Guo, L. Xiong, C. Zhao, M. Qu, L.I. Escano, X. Xiao, K. Fezzaa, W. Everhart, T. Sun, L. Chen, *Nat. Commun.* **10**, 1 (2019).
22. R. Cunningham, C. Zhao, N. Parab, C. Kantzos, J. Pauza, K. Fezzaa, T. Sun, A.D. Rollett, *Science* 80, **363**, 849 (2019).
23. A.A. Martin, N.P. Calta, J.A. Hammons, S.A. Khairallah, M.H. Nielsen, R.M. Shuttlesworth, N. Sinclair, M.J. Matthews, J.R. Jeffries, T.M. Willey, J.R.I. Lee, *Mater. Today Adv.* **1**, 100002 (2019).
24. S.A. Khairallah, A.A. Martin, J.R.I. Lee, G. Guss, N.P. Calta, J.A. Hammons, M.H. Nielsen, K. Chaput, E. Schwalbach, M.N. Shah, M.G. Chapman, T.M. Willey, A.M. Rubenchik, A.T. Anderson, Y. Morris Wang, M.J. Matthews, W.E. King, *Science* 80, (**368**), 660 (2020).
25. A.A. Martin, N.P. Calta, S.A. Khairallah, J. Wang, P.J. Depond, A.Y. Fong, V. Thampy, G.M. Guss, A.M. Kiss, K.H. Stone, C.J. Tassone, J. Nelson Weker, M.F. Toney, T. van Buuren, M.J. Matthews, *Nat. Commun.* **10**, 1 (2019).
26. C.L.A. Leung, S. Marussi, M. Towrie, J. del Val Garcia, R.C. Atwood, A.J. Bodey, J.R. Jones, P.J. Withers, P.D. Lee, *Addit. Manuf.* **24**, 647 (2018).
27. P.-J. Chiang, R. Jiang, R. Cunningham, N. Parab, C. Zhao, K. Fezzaa, T. Sun, A.D. Rollett, in *Advanced Real Time Imaging II*, The Minerals, Metals & Materials Series, J. Nakano, P.C. Pistorius, C. Tamerler, H. Yasuda, Z. Zhang, N. Dogan, W. Wang, N. Saito, B. Webler, Eds. (Springer, Cham, Switzerland, 2019), pp. 77–85.
28. N. Kouraytem, X. Li, R. Cunningham, C. Zhao, N. Parab, T. Sun, A.D. Rollett, A.D. Spear, W. Tan, *Phys. Rev. Appl.* **11**, 1 (2019).

29. Q. Guo, C. Zhao, M. Qu, L. Xiong, S.M.H. Hojjatzadeh, L.I. Escano, N.D. Parab, K. Fezzaa, T. Sun, L. Chen, *Addit. Manuf.* **31**, 100939 (2020).
30. C. Zhao, Q. Guo, X. Li, N. Parab, K. Fezzaa, W. Tan, L. Chen, T. Sun, *Phys. Rev. X* **9**, 21052 (2019).
31. X. Li, C. Zhao, T. Sun, W. Tan, *Addit. Manuf.* **101362**, (2020).
32. A.J. Clarke, D. Tourret, Y. Song, S.D. Imhoff, P.J. Gibbs, J.W. Gibbs, K. Fezzaa, A. Karma, *Acta Mater.* **129**, 203 (2017).
33. G. Reinhart, C.A. Gandin, N. Mangelinck-Noël, H. Nguyen-Thi, B. Billia, J. Baruchel, *IOP Conf. Ser. Mater. Sci. Eng.* **33**, 0 (2012).
34. B. Gould, S. Wolff, N. Parab, C. Zhao, C. Lorenzo-Martin, K. Fezzaa, A. Greco, T. Sun, *JOM* (2020), https://doi.org/10.1007/s11837-020-04291-5.
35. N.H. Paulson, B. Gould, S.J. Wolff, M. Stan, A.C. Greco, *Addit. Manuf.* **34** (2020).
36. S. Shevchik, T. Le-Quang, B. Meylan, F.V. Farahani, M.P. Olbinado, A. Rack, G. Masinelli, C. Leinenbach, K. Wasmer, *Sci. Rep.* **10**, 3389 (2020).
37. S.J. Wolff, H. Wu, N. Parab, C. Zhao, K.F. Ehmann, T. Sun, J. Cao, *Sci. Rep.* **9**, 1 (2019).
38. S. Webster, S. Wolff, J. Bennett, T. Sun, J. Cao, K. Ehmann, *Microsc. Microanal.* **25**, 2556 (2019).
39. N.D. Parab, J.E. Barnes, C. Zhao, R.W. Cunningham, K. Fezzaa, A.D. Rollett, T. Sun, *Sci. Rep.* **9**, 1 (2019).
40. T. Sun, K. Fezzaa, *J. Synchrotron Radiat.* **23**, 1046 (2016).
41. J. Glerum, T. Sun, C. Kenel, D.C. Dunand, *Addit. Manuf.* **36**, 101461 (2020).
42. N.P. Calta, J. Wang, A.M. Kiss, A.A. Martin, P.J. Depond, G.M. Guss, V. Thampy, A.Y. Fong, J.N. Weker, K.H. Stone, C.J. Tassone, M.J. Kramer, M.F. Toney, A. Van Buuren, M.J. Matthews, *Rev. Sci. Instrum.* **89** (2018).
43. A.M. Kiss, A.Y. Fong, N.P. Calta, V. Thampy, A.A. Martin, P.J. Depond, J. Wang, M.J. Matthews, R.T. Ott, C.J. Tassone, K.H. Stone, M.J. Kramer, A. van Buuren, M.F. Toney, J. Nelson Weker, *Adv. Eng. Mater.* **21**, 1 (2019).
44. V. Thampy, A.Y. Fong, N.P. Calta, J. Wang, A.A. Martin, P.J. Depond, A.M. Kiss, G. Guss, Q. Xing, R.T. Ott, A. van Buuren, M.F. Toney, J.N. Weker, M.J. Kramer, M.J. Matthews, C.J. Tassone, K.H. Stone, *Sci. Rep.* **10**, 1 (2020).
45. C.L.A. Leung, S. Marussi, R.C. Atwood, M. Towrie, P.J. Withers, P.D. Lee, *Nat. Commun.* **9**, 1 (2018).
46. C.L.A. Leung, S. Marussi, M. Towrie, R.C. Atwood, P.J. Withers, P.D. Lee, *Acta Mater.* **166**, 294 (2019).
47. Y. Chen, S.J. Clark, C.L.A. Leung, L. Sinclair, S. Marussi, M.P. Olbinado, E. Boller, A. Rack, I. Todd, P.D. Lee, *Appl. Mater. Today* **20**, 100650 (2020).
48. S. Hocine, S. Van Petegem, U. Frommherz, G. Tinti, N. Casati, D. Grolimund, H. Van Swygenhoven, *Addit. Manuf.* 101194 (2020).
49. S. Hocine, H. Van Swygenhoven, S. Van Petegem, C.S.T. Chang, T. Maimaitiyili, G. Tinti, D. Ferreira Sanchez, D. Grolimund, N. Casati, *Mater. Today* **34**, 30 (2019).
50. C. Kenel, D. Grolimund, X. Li, E. Panepucci, V.A. Samson, D.F. Sanchez, F. Marone, C. Leinenbach, *Sci. Rep.* **7**, 1 (2017).
51. J. Filik, A.W. Ashton, P.C.Y. Chang, P.A. Chater, S.J. Day, M. Drakopoulos, M.W. Gerring, M.L. Hart, O. V. Magdysyuk, S. Michalik, A. Smith, C.C. Tang, N.J. Terrill, M.T. Wharmby, H. Wilhelm, *J. Appl. Crystallogr.* **50**, 959 (2017). □

Tao Sun has been an associate professor in the Department of Materials Science and Engineering at University of Virginia since 2019. Previously, he served as a beamline scientist at the Advanced Photon Source of Argonne National Laboratory. He received his BS and MS degrees in materials science and engineering from Tsinghua University, China, and his PhD degree from Northwestern University. His research focuses on studying additive manufacturing processes and materials using synchrotron x-ray and other *in situ*/*ex situ* characterization tools. Sun can be reached by email at ts7qw@virginia.edu.

Wenda Tan is an assistant professor in the Department of Mechanical Engineering at the University of Utah. He received his BS and MS degrees in mechanical engineering from Tsinghua University, China, and his PhD degree in mechanical engineering from Purdue University. His research focuses on computational heat transfer, computational fluid mechanics, computational materials and their applications in various advanced manufacturing techniques, such as additive manufacturing, welding and joining, and casting. His awards include the National Science Foundation CAREER Award in 2018. Tan can be reached by email at wenda.tan@mech.utah.edu.

Lianyi Chen is an assistant professor in the Department of Mechanical Engineering at the University of Wisconsin-Madison. He received PhD degree in materials science and engineering from Zhejiang University, China. His research includes four highly interrelated research areas: metal additive manufacturing, metals design based on nanoelements, smart metal manufacturing, and *in situ*/*in operando* characterization. He has published more than 70 journal papers, and is an inventor with seven patents (two licensed). Chen can be reached by email at lianyi.chen@wisc.edu.

Anthony Rollett has been the U. S. Steel Professor in Materials Science and Engineering at Carnegie Mellon University (CMU). He received PhD degree in materials engineering from Drexel University. He previously worked at the Los Alamos National Laboratory (LANL) for sixteen years. He was the Deputy Division Director of Materials Science and Technology in LANL before taking the department head position in CMU in 1995. His awards include a Fellow of The Minerals, Metals & Materials Society in 2011, and an International Francqui Professor for 2020–2021, Belgium. He is a co-Director of the Next Manufacturing Center at CMU and is a leader in research and education in additive manufacturing. Rollett can be reached by email at rollett@andrew.cmu.edu.